THE JOURNAL OF PHYSICAL CHEMISTRY C

Article

Cite This: J. Phys. Chem. C 2019, 123, 8975−8982

pubs.acs.org/JPCC

Directing Long-Range Molecular Ordering in Ionic Liquid Films: A Tale of Two Interfaces

Radhika S. Anaredy* and Scott K. Shaw*

Department of Chemistry, University of Iowa, Iowa City, Iowa 52242, United States

Supporting Information

ABSTRACT: We report surface-dependent, long-range ordering behavior of two ionic liquids, 1-butyl-1-methylpyrrolidinium tetracyanoborate (P14 $B(CN)_4$) and 1-butyl-1-methylpyrrolidinium dicyanamide (P14 $N(CN)_2$). The ionic liquids are supported as liquid films and examined using vibrational spectroscopy and spectroscopic ellipsometry. Both systems show changes in the infrared peak profile characteristic of major dipole reorientations for both anions, but the changes observed are in different spectral regions. Specifically, tetracyanoborate shows changes in the B−C stretching modes, and dicyanamide displays changes in the C≡N and N−C modes. Surprisingly, $B(CN)_4$ induces a final film environment, which is identical to the solid−liquid interfacial orientation. However, the $N(CN)_2$ indicates propagation of the gas−liquid interfacial environment through the film toward the solid substrate. The extent of ordering within the films extends to 0.4 and 1.1 μm for P14 $N(CN)_2$ and P14 $B(CN)_4$, respectively. This observation is intriguing as it presents a possibility for controlling molecular (re)orientations at 100 s of nanometer scales by tuning fundamental intermolecular interactions at surfaces. These results for the cyano-functionalized anions should be generally applied for other systems, contributing directly to a better understanding and design for applications in molecular electronics, lubrication, and energy storage devices.

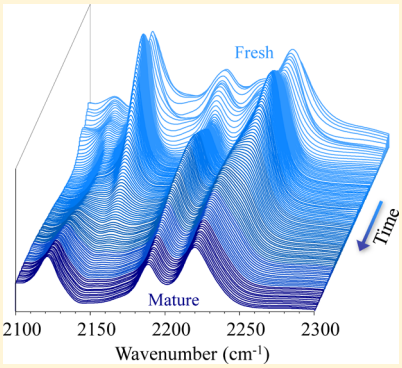

INTRODUCTION

Advantageous properties such as low vapor pressure, moderate conductivity, high thermal and chemical stability, and low flammability have inspired diverse utility for ionic liquids (ILs).[1−3] Commercial demands for increased performance in these applications and a desire for fundamental understanding of physicochemical properties require detailed investigations of interfacial and thin film behaviors. This is particularly true for IL intriguing intermolecular architectures that have been reported in the bulk phase and near surfaces. In particular, the unique structures and behaviors of ILs at solid−liquid interfaces govern their applications in the fields of electrochemistry, catalysis, and lubrication.[4−7] The incredible diversity of possible IL compositions and the corresponding range of attributes possible at the solid−liquid interface motivates the need for a fundamental understanding of these ionic solvents to develop a general model to predict and tune the interfacial molecular structures and behaviors.

Investigations of ionic liquid unique ordering behaviors are not a new area. Several previous computational and experimental studies show nanoscale domains of polar and nonpolar groups that permeate the bulk liquid. The relative size of these domains depends on tunable parameters including the cation (a)symmetry, alkyl chain length, and temperature.[8−12] Other studies suggest that molecular ordering of the IL extends only single nanometers from a surface and does not permeate the bulk.[5,13−15] AFM and angle-resolved X-ray photoelectron spectroscopy studies done on thin films of ILs show alternating layers of cations and anions on a mica surface up to a thickness of 0.41 nm beyond, which a sponge-like structure is observed.[16] Similar layered structure formed by a different IL is shown to extend to 17 nm on a mica surface at a relative humidity of 45% as water facilitates displacement of K^+ ions on a mica surface, thus rendering the surface negatively charged, which allows the cation to initiate the layering.[17] A surface force apparatus has been used to confine IL films between two parallel surfaces and analyzing the film behavior under a shear, which is applied by sliding the two surfaces over each other. Previous work using this technique has shown transition of a liquid film to a solid-like structure as the surfaces are brought closer to each other.[18−22] These solid-like films have viscosities of 1−3 orders of magnitude higher than bulk but lower than their glass phase, thus retaining their mobility.[21] The above-described studies display effect of various factors such as surface-film interaction, impurity, and shear on the behavior of IL films. Our previous work investigated IL behavior under the influence of a flow-induced shear and depicted formation of long-range-ordered structures that extended up to few micrometers unlike the above-described studies.[23] More recent reports show ordering that ranges from tens to hundreds of nanometers away from a planar surface.[4,23−27] A few specific examples that are most relevant

Received: December 31, 2018
Revised: March 13, 2019
Published: March 13, 2019

DOI: 10.1021/acs.jpcc.8b12575
J. Phys. Chem. C 2019, 123, 8975−8982

to our work reported here include 1-hexyl-3-methylimidazolium ethylsulfate alternating between liquid- and solid-like structures that propagate 60 nm from a solid surface under the influence of the shear and nanoconfinement.[26] A computational study shows that, upon introduction of vacuum interfaces on either side of an IL bath, the sponge-like morphology frequently observed in bulk ILs converted to lamellar structures that extends across the full simulation slab (10 nm).[4] Ionic liquids need not to be confined by a planar surface to show evidence of ordering. One study of supported ionic liquid membranes (SILMs) shows that the orientational relaxation of molecules such as $SeCN^-$ and CO_2 is much slower in SILMs (pore sizes of 100 to 350 nm) than they are in the bulk ILs, implying that that even significantly curved pore walls can influence the IL structure at distances of more than hundred nanometers.[28] Recent 2D infrared spectroscopy studies on IL films supported on a solid substrate also showed that the influence of the solid surface could be longer ranged in ILs as compared to molecular fluids.[29]

The behavior of cyano-functionalized ILs in thin films and interfaces is particularly interesting for several technological applications, including their potential in dye-sensitized solar cells.[30,31] The electrochemical and thermal stability, low viscosity, and donor-type solvent properties of dicyanamide ILs make them excellent solvents for organic and inorganic compounds.[32] In one report, four ILs with imidazolium cations and cyano-functionalized anions (tetracyanomethanide (TCM), tetracyanoborate (TCB), dicyanamide (DCA), and thiocyanate (SCN)) are studied using vibrational spectroscopy.[33] FTIR and Raman were used to assign vibrational peak profiles for bulk fluids, whereas vSFG was used to elucidate the structure at gas−liquid interfaces. Orientational analysis of C−H stretching peaks in the vSFG spectra supports a model wherein the cation resides at the vapor interface, the imidazolium ring lies in the plane of the surface, and the alkyl chain points out of the liquid into the gas phase much like a typical surfactant. The cation orientation is not affected by changing anions, and three of four ILs investigated show intensity in the C≡N stretching region, with SCN^- being the exception.[33] The lack of the C≡N vibration intensity indicates that either SCN^- is excluded from the interfacial region or the vibration dipole is not orientated to be surface active.[33] The second study on the same set of ILs at the solid−liquid interface was carried out at the IL-NaCl(100) and IL-BaF_2(111) surfaces. A strong interaction is reported between the NaCl(100) surface and the cation, whereas BaF_2(111) generally shows stronger interaction with the anions. EMIM TCB is an exception that shows a stronger interaction between the BaF_2(111) surface and a strongly ordered adjacent cation layer, and the TCB anion leads to anion overcrowding.[34] On the basis of our earlier work[35] and the interaction of cyano-functional groups with metals,[36,37] we predicted that the cyano-based ILs might exhibit enhanced ordering of the ionic liquid near our metallic surfaces leading to the template-ordered growth of an ordered liquid layer from the solid substrate into the bulk fluid. If true, this would be observable by observing ordered structures that persist into the IL bulk phase and are identical to those immediately adjacent to the metallic substrate. Here, we report results of our study to investigate this hypothesis using 1-butyl-1-methylpyrrolidinium tetracyanoborate and 1-butyl-1-methylpyrrolidinium dicyanamide.

EXPERIMENTAL SECTION

Materials. 14 mm polycrystalline silver discs are used as the solid substrate for all measurements. These discs are cut from a silver rod (99.999% purity) purchased from ESPI Metals, Portland, OR. The substrates are mechanically polished using 600 and 1000 grit sandpapers followed by 9.5, 3.0, 1.0, and 0.3 μm alumina powder on polishing pads (Buehler) to obtain a mirror finish. Before each experiment, the substrates are subjected to a chemical polishing step, which includes H_2SO_4 (ACS grade, BDH), $HClO_4$ (70%, Sigma), and NH_4OH (28 to 30%, BDH) as received, along with an aqueous solution of 4 M CrO_3 (99.9%, Aldrich) and 0.6 M HCl (ACS grade, BDH) as described previously.[38] All solutions are prepared using ultrapure water (18.2 MΩ cm with TOC ≤ 4 ppb) generated by a Milli-Q UV Plus system (Millipore Corp). The quality of the Ag surfaces is characterized for roughness and cleanliness, determined by AFM and ellipsometry, respectively. The RMS roughness of the surfaces over an area of 1 × 1 μm is found to be <5 nm, and the substrate optical constants are in agreement with literature values for bare silver.[39] 1-butyl-1-methylpyrrolidinium tetracyanoborate (P14 $B(CN)_4$) and 1-butyl-1-methylpyrrolidinium dicyanamide (P14 $N(CN)_2$) (Merck KGaA in Darmstadt, Germany) are dried under vacuum at 60 °C for >24 h and stored under dry conditions in a glove box (Genesis, Vacuum Atmospheres Company) with O_2 and H_2O levels of <0.5 and < 10 ppm, respectively. The water content of the ILs is monitored periodically via KF titration and was found to be 400 ± 200 ppm. The amounts of water measured in individual IL samples do not have a significant effect on the results reported here.

Instrumental Methods. *Dynamic Wetting.* The technique creates IL films on silver substrates in a custom-made airtight PTFE cell as described in our previous report.[23] In brief, the substrate is affixed to a brass rod, which in turn is attached to a gearhead and electric motor assembly that provides rotation of the substrate at a controlled but variable velocity. This assembly is inserted in the PTFE cell, which is purged continuously with an inert gas to protect the sample from atmospheric moisture and gases. Inside this cell, IL films are made by rotating the Ag substrate through a droplet of the IL fluid, which is held between the substrate and a capillary. The PTFE cell is equipped with two UV grade CaF_2 windows (Casix, U.K.) on either side of the substrate allowing entry and exit of the incident and reflected beams.

Fourier Transform Infrared Spectroscopy (FTIR). A Thermo-Nicolet iS50 Fourier transform infrared spectrometer with a liquid nitrogen cooled an MCT-A detector acquires FTIR spectra of bulk fluid. Measurements use approximately 2 μL of the fluids pressed between CaF_2 windows. Spectra are obtained at a resolution of 4 cm^{-1} with an optical velocity of 1.8988 and are averaged over 128 scans.

Infrared Reflection Absorption Spectroscopy (IRRAS). All IRRAS spectra are acquired in the wetting cell (described above) on an enclosed external optical bench, which is purged with dry and CO_2 free air. The IR beam from the FTIR spectrometer is directed to the external bench where it passes through a wire grid polarizer to obtain a p-polarized IR beam, which impinges the sample at a grazing angle. A freshly cleaned and dry Ag surface is used to obtain background spectra in the same geometry. The selection rules of IRRAS and p-polarized light source allow the technique to probe vibrational modes with a portion of a dipole moment perpendicular to the Ag

DOI: 10.1021/acs.jpcc.8b12575
J. Phys. Chem. C 2019, 123, 8975−8982

surface. IRRAS spectra shown in this work are averaged over 1000 scans acquired at a 4 cm^{-1} resolution and an optical velocity of 1.8988.

Spectroscopic Ellipsometry. A M-2000 V spectroscopic ellipsometer (J.A. Woollam) is used to determine optical constants and film thickness from the ψ and Δ values reported as a function of wavelength. The thickness of IL films made by the above-described wetting technique is determined as a function of time by fitting the ψ and Δ values obtained at different time points with an appropriate model in the CompleteEase software. The model used in this study consists of a bare substrate (silver), an intermix layer, and a general oscillator layer that takes into consideration any small absorptions by the film.

RESULTS AND DISCUSSION

Figure 1 shows IR absorption spectra for P14 $N(CN)_2$ under three different experimental conditions. The top (black) trace

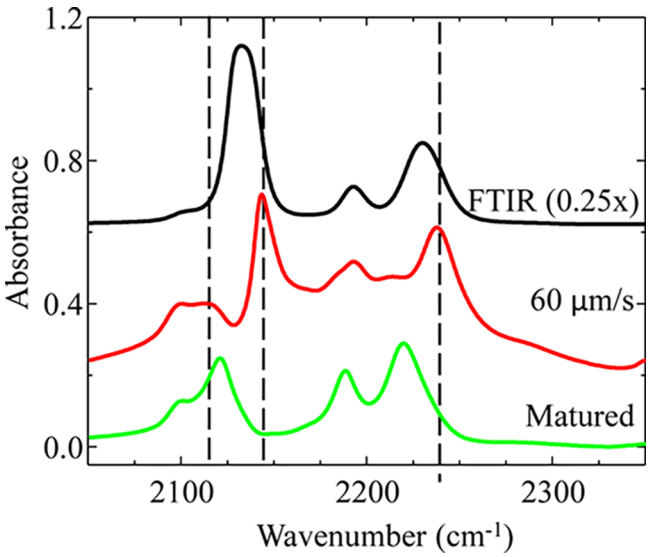

Figure 1. FTIR and two IRRAS spectra of 1-butyl-1-methylpyrrolidinium dicyanamide are compared. The top (black) trace is the FTIR spectra representing the bulk isotropic liquid. The middle (red) trace is the IRRAS spectra acquired from a freshly prepared film while the surface is rotated at a velocity of 60 μm/s. The bottom (green) trace is the IRRAS spectra of the same film after it has matured for 900 ± 200 min after a substrate rotation is stopped. Vertical dashed lines indicate key changes that occur as the film matures. The FTIR data has been scaled (0.25×) to fit on the same absorbance axis as the IRRAS data. The spectra are vertically offset for clarity.

shows a transmission FTIR spectrum of the bulk fluid, representing the IL in its bulk, or isotropic, state. The middle (red) trace is an IRRAS spectrum, acquired as the IL film spreads across an Ag surface being rotated at a constant velocity (60 μm/s). The bottom (green) trace in Figure 1 represents IRRAS data from a matured film, which is left motionless (no substrate rotation). The film maturation begins when the substrate rotation is stopped and, for P14 $N(CN)_2$, continues for 900 ± 200 mins. A comparison of the bulk transmission FTIR spectra (black) to the rotating IRRAS spectrum (red) shows multiple absorption features for the same vibrational modes and frequency shifts in the existing peaks. We attribute these changes from the "bulk" absorption profile to the creation of new different chemical environments within the freshly prepared film, which the IRRAS technique is able to distinguish here.[35] The differences between the fresh and matured IRRAS spectra represent changes in a chemical environment and a molecular reorientation after the substrate rotation is stopped. The maturation time allows the IL molecules within the film to organize themselves over great distances, and the organization is tracked, in this case, by interpreting major differences in the C≡N stretching region, which extends from approximately 2075 to 2250 cm^{-1}.[33] Three major changes are observed as a function of time as the fresh film (red) matures to its final state (green). These are noted with vertical dashed lines in Figure 1, which are (from left to right) (1) the peak at 2114 cm^{-1} shifts to 2121 cm^{-1}, (2) the peak at 2144 cm^{-1} loses its intensity completely, and (3) the peak at 2238 cm^{-1} shifts to 2220 cm^{-1}. In addition to the C≡N stretching peaks, the peak corresponding to the N−C asymmetric stretching mode also shows a shift from 1312 to 1299 cm^{-1} as a function of film maturation (Figure S1). The freshly prepared film (red) shows multiple peaks arising from the same molecular vibration, suggesting the presence of discrete chemical environments within the film volume. When the substrate rotation is stopped, the molecules in the film continue to flow slowly yielding a shearing effect on the film against the solid substrate. Along with an overall decrease in film thickness, the shearing and intermolecular forces direct a significant reorganization of the IL anions to a favored state. This is clearly evident from the evolution of a single peak for each vibrational mode in the matured (green) spectrum unlike a fresh film spectrum (red). We refer to this process as "film maturation". Because the changes discussed above occur in the anion peaks, the maturation process is mainly characterized by reorganization of the anions. It is also important to note that the matured spectrum exhibits peaks in the C≡N and N−C stretching regions, which are completely different from the freshly prepared film. This implies that the chemical environment acquired by the matured film is very different from those existing in the freshly prepared film or in the bulk phase.

Figure 2 shows infrared absorption spectra under the same conditions as described previously but for the ionic liquid P14 $B(CN)_4$. The top black trace is the transmission FTIR spectrum for the bulk liquid with an isotropic molecular orientation. The middle red trace is the IRRAS spectrum for a freshly prepared IL film, acquired as the surface rotates at a velocity of 60 μm/s. The bottom green trace is the IRRAS spectrum for the same film acquired 70 min after the substrate rotation is completely stopped. The order of magnitude change in maturation times for these liquids (900 vs 70 min.) in spite of the small difference in their viscosity (P14 $N(CN)_2$:41 cP and P14 $B(CN)_4$:52 cP) is attributed to differences in the anion volumes calculated to be 116.93 $Å^3$ for $B(CN)_4$ versus 63.78 $Å^3$ for $N(CN)_2$. A larger size to charge ratio leads to weaker interactions with the cation because of delocalization of the anion negative charge over a higher volume. This allows the anion to move more freely of the cation. Major differences in the fresh (red) and mature (green) spectra are seen in the lower frequency region from 900 to 1000 cm^{-1} and highlighted with a vertical dashed line. The transmission FTIR spectrum shows a single peak at 933 cm^{-1} representing the B−C stretch, whereas the IRRAS spectrum representing the freshly prepared film shows a peak and a shoulder at 950 and 927 cm^{-1}, respectively. The presence of two peaks in this region indicates the presence of two different environments where the B−C bonds are interacting in different ways within the same film.

DOI: 10.1021/acs.jpcc.8b12575
J. Phys. Chem. C 2019, 123, 8975−8982

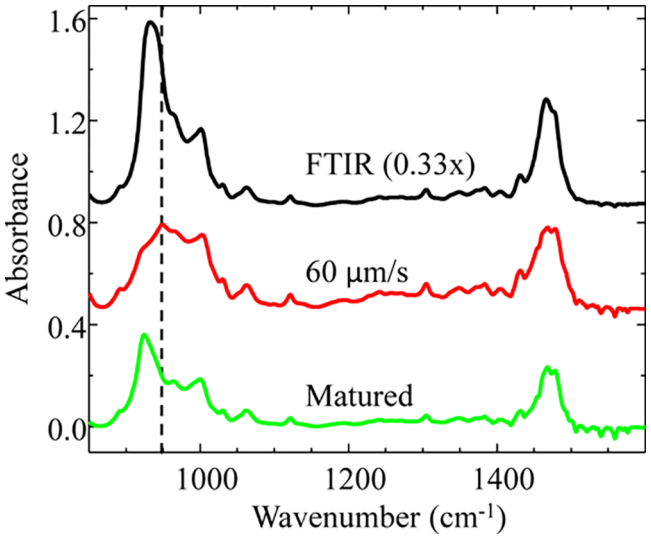

Figure 2. FTIR and two IRRAS spectra of 1-butyl-1-methylpyrrolidinium tetracyanoborate are compared. The top (black) trace is the FTIR spectra representing the bulk isotropic liquid. The middle (red) trace is the IRRAS spectra acquired from a freshly prepared film while the surface is rotated at a velocity of 60 μm/s. The bottom (green) trace is the IRRAS spectra of the same film after it has matured for 70 ± 10 min after a substrate rotation is stopped. Vertical dashed lines indicate key changes that occur as the film matures. The FTIR data has been scaled (0.33×) to fit on the same absorbance axis as the IRRAS data. The spectra are vertically offset for clarity.

Comparison between the two IRRAS spectra (red and green) also shows significant changes in the B−C stretching peak. Similar to the $N(CN)_2$ anion, we interpret these results for $B(CN)_4$ to indicate the presence of two distinct different environments in the film, which our IRRAS measurements are capable of resolving. During the film maturation, the peak at 950 cm^{-1} loses its intensity, whereas the shoulder at 927 cm^{-1} grows into a well-defined peak. These changes in the spectral profile over a period of 70 min imply a corresponding shift of the prevalent chemical environment.

Both ILs studied here contain the same P14 cation. The consistent peak profile of the cation (C−H stretching peaks at higher frequencies and the peaks corresponding to the ring in 1600−1400 cm^{-1}) suggests that the cation does not change its average molecular orientation nor does it experience any significant difference in a chemical environment. The intensity of cation peaks decreases (but do not shift) after the substrate rotation is stopped because of film thinning (see thickness values reported in Figure S2). However, the absorbance bands of the cation modes do not sharpen or shift, which indicates the material remains in the liquid phase throughout the maturation process.[40]

Table 1 shows assignments for the peaks that undergo changes with time as the film matures in both ILs.[34,41−43] FTIR and matured IRRAS spectra of each IL depict the same number of peaks in the IR region of interest, but significant shifts in the peak frequencies are observed. This implies that chemical environments in the matured film are different from the isotropic bulk. Also, the absence of additional peaks in IRRAS spectra of matured films compared to that of freshly prepared film indicates significant uniformity in a chemical environment in the 'matured' film.

Both ILs used in this study consist of cyano-functionalized anions, but in case of P14 $B(CN)_4$, no change is observed in the C≡N stretching peak (Figure S3), whereas in P14 $N(CN)_2$, major changes are observed only in the C≡N stretching region (Table 1). The discrepancy in the behavior of these two anions, despite having the common cyano group, could be attributed to one or more of the following factors: (i) the interaction of the two anions with the metal surface could be very different as $B(CN)_4$ can interact with the surface through nitrogens in the nitrile group, whereas $N(CN)_2$ has two different types of nitrogens (nitrogens from the nitrile group and the amide nitrogen) available that could participate in the interactions and (ii) both anions have different geometries ($B(CN)_4$ is tetrahedral and $N(CN)_2$ is bent), and the charge is delocalized over a larger area in the case of $B(CN)_4$ as compared to $N(CN)_2$. All these factors not only influence their interactions with the metal surface but also affect intermolecular interactions, thus resulting in a very different response from the two anions under similar conditions. Because $B(CN)_4$ is a symmetrical anion, no changes in the molecular orientation are expected. However, a change in the B−C stretch of the anion is observed as a function of time. This is attributed to changes in the chemical environment resulting from an increasingly confined environment that affects each of the quaternary CN groups equally.

Table 1. Lists of Vibrational Energies in Wavenumber (cm^{-1}) and Assignments for Key Absorbance Features of the Ionic Liquids Probed Here in Bulk Phase (FTIR) and in IRRAS during Rotation and after Maturation[27,35−37]

	P14 $B(CN)_4$		
assignments	FTIR	IRRAS (rotating)	IRRAS (matured)
B−C stretch	934	950 & 927	927
	P14 $N(CN)_2$		
assignments	FTIR	IRRAS (rotating)	IRRAS (matured)
C≡N asym stretch	2133	2114	2121
		2144	
C≡N sym stretch	2191	2193	2189
C≡N comb stretch		2213	
	2228	2238	2220
N−C asym stretch	1306	1312	1299

Figures 3 and 4 show a series of IRRAS spectra that detail the gradual changes to spectral features as the films mature. When the substrate rotation is stopped, the film slowly flows and thins under the influence of gravity. This is shown by the continuously decreasing thickness (Figure S2) as tracked by spectroscopic ellipsometry. As mentioned, significant changes are also observed in the peak profiles of these spectra illustrated by the dashed lines in the two figures. Figures S4 and S5 show the shift in the IR peak frequencies (2238 and 2113 cm^{-1} for $N(CN)_2$ and 948 cm^{-1} for $B(CN)_4$) for the two ILs as a function of time. We assign the changes in the absorption peak profiles to anion reorganization facilitated by the flowing film, ultimately leading to significant changes in a chemical environment and a long-ranging-ordered structure as suggested previously.[23,35] The maturation process is considered complete when the peak profile of the film appears constant over consecutive time points, even though the peak intensities decrease due to thinning of the film as it continues to flow under the influence of gravity. This decrease in intensity of the entire absorption profile is important as it proves that the IL remains a liquid throughout (and after) the maturation process. Also important is the complete reversi-

DOI: 10.1021/acs.jpcc.8b12575
J. Phys. Chem. C 2019, 123, 8975−8982

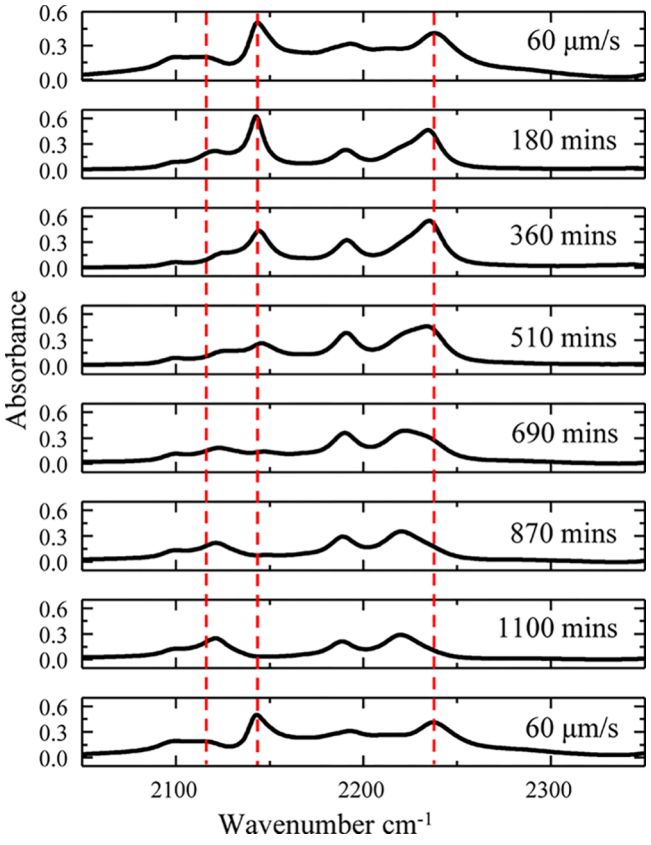

Figure 3. Set of IRRAS spectra of P14 $N(CN)_2$ showing changes in the spectral profile as a function of time. The top spectra correspond to the freshly prepared film while the substrate is rotating at a velocity of 60 μm/s. The next six spectra represent the same film after a substrate rotation is stopped. The last spectra represent the film obtained on replenishing the matured film by bulk drop, that is, by rotating the film at the same speed as before.

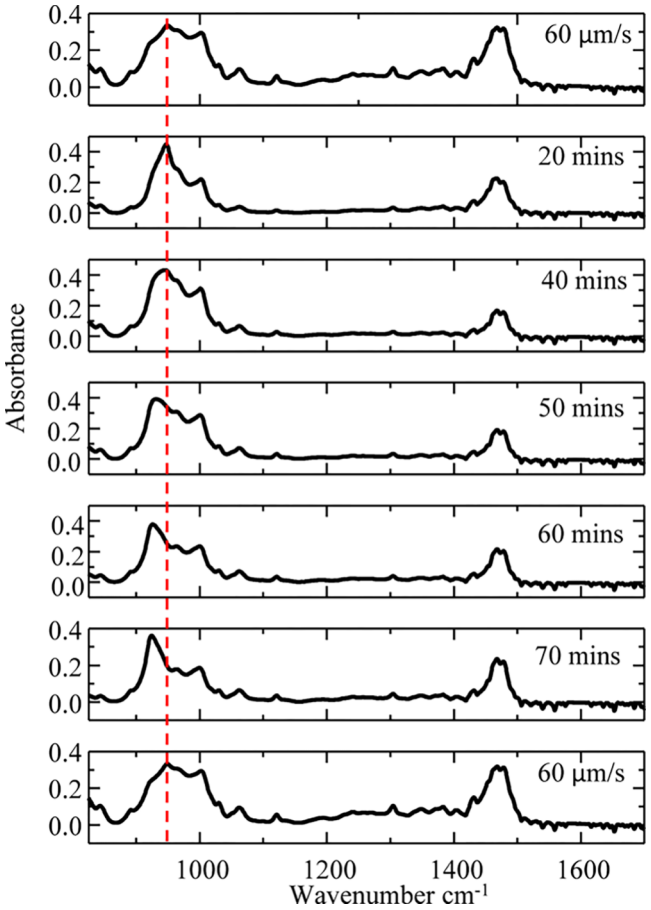

Figure 4. Set of IRRAS spectra of P14 $B(CN)_4$ showing changes in the spectral profile as a function of time. The top spectra correspond to the freshly prepared film while the substrate is rotating at a velocity of 60 μm/s. The next five spectra represent the same film after a substrate rotation is stopped. The last spectra represent the film obtained on replenishing the matured film by bulk drop, that is, by rotating the film at the same speed as before.

bility of the maturation process; the initial (top) and final (bottom) spectra shown in Figures 3 and 4 are identical, demonstrating complete reversibility of the maturation process and ensuring the change is purely physical. This eliminates the possibility of any chemical change or contamination of the system during the long time required for these measurements. Importantly, the film thicknesses of the matured films are 0.4 and 1.1 μm for P14 $N(CN)_2$ and P14 $B(CN)_4$, respectively. These thicknesses are much higher than previously reported interfacial films, showing the process occurring here is fundamentally different from typical interfacial structuring.[5,13,14,25,27,44] To confirm that the observation corresponds to the entire thickness of the film, that is, our IRRAS measurements are probing the entire film thickness, additional experiments are carried out for both the ILs wherein the rotational speed of the substrate (and hence IL film thickness) is systematically varied. These experiments (Figure S6) show clear correlations in IR absorbance with a substrate velocity, confirming the observed range of ordering.

Table 2 lists the C≡N stretching peaks obtained for P14 $N(CN)_2$ using IRRAS with those observed in SFG spectra for BMIM $N(CN)_2$ at the gas–liquid and IL-BaF_2 interface.[33,34] As mentioned earlier, the IRRAS spectrum of a freshly prepared film exhibits more than one peak for the same vibrational mode in the C≡N stretching region, indicating multiple chemical environments are present within the film

Table 2. Comparison of C≡N Stretching Peak Energies (cm^{-1}) Observed for P14 $N(CN)_2$ in IRRAS with SFG Results Obtained for BMIM $N(CN)_2$ in the Same Region at Gas–Liquid and IL-BaF_2 Interface[a]

	P14 $N(CN)_2$			BMIM $N(CN)_2$	
assignment	FTIR	IRRAS (rotating)	IRRAS (matured)	SFG IL-BaF_2	SFG gas–liq
C≡N asym stretch	2133	2113	**2121**		**2125**
		2144*		2145*	
C≡N sym stretch	2191	2193*	**2189**	2194*	**2185**
C≡N comb stretch		2213			
	2228	2238*	**2220**	2242*	**2218**

[a]SFG data are from refs 33 and 34.

volume. One set of peaks in the IRRAS spectra of the freshly prepared film resembles the peaks observed in SFG spectra in their frequencies at the IL-BaF_2 interface as noted with asterisks in Table 2.[34] On the other hand, the peak frequencies in the matured film spectra resemble peaks in the SFG spectra obtained from the gas–liquid interface (bold black in Table 2).[33] On the basis of the similarity in peak energies between these two vSFG spectra[33,34] with our own IRRAS data

DOI: 10.1021/acs.jpcc.8b12575
J. Phys. Chem. C 2019, 123, 8975–8982

acquired for films under different conditions, we propose that some molecules in our freshly prepared film adopt an orientation that matches closely that of the solid surface. This indicates that the second absorption feature for the same vibrational mode, which we find in our IRRAS data, likely represents IL molecules farther away from the surface in the volume between the solid−liquid interface and the gas−liquid interface. Further, on the basis of the similarity between our IRRAS data and the vSFG data for the gas−liquid interface,[33] we propose that the maturation process involves the entirety of our IL film adopting the molecular arrangement found at the gas−liquid interface. This orientation likely grows to propagate throughout the film while the film is still flowing, giving rise to peak frequencies in the matured film spectra that resemble the SFG peak frequencies for the same modes at the gas−liquid interface.[33] This indicates that the molecular organization at the gas−liquid interface is ultimately favored over the initial solid−liquid interface. A recent AFM study on IL nanodroplets shows evidence of nanodroplets spreading over a course of hours to form a layered structure because of weak interaction of the IL with mica at low humidity.[45] This observation indicates that the stable solid-like structure formed at the solid−liquid interface is mobile and capable of changing over time based on the experimental conditions as also evidenced by above-described results on P14 $N(CN)_2$ where the matured film resembles the gas−liquid interfacial arrangement.

The IRRAS spectra for P14 $B(CN)_4$ obtained for a freshly prepared film also display more than one peak for the same vibrational mode, indicating multiple chemical environments. The changes observed in the IRRAS spectra as a function of time indicate significant changes to the local molecular environment. The key feature in the IRRAS spectra that support this change is apparent between approximately 920 and 1000 cm^{-1}. Specifically, a strong absorbance band at 935 cm^{-1} is present in the FTIR spectrum corresponding to the B−C stretching mode. The IRRAS spectrum for the freshly prepared film depicts two features (a peak at 950 cm^{-1} and a shoulder at 927 cm^{-1}) for the B−C stretching mode, whereas the IRRAS spectrum of the matured film shows a well-defined peak at 927 cm^{-1}. As mentioned earlier, the peak at 950 cm^{-1} loses intensity, whereas the feature at 927 cm^{-1} grows into a well-defined peak as the film matures. The decrease in absorbance at 950 cm^{-1} as the film matures indicates that the chemical environment that induces the lower energy vibration is energetically favored and that this environment spreads throughout the entire film over the maturation time. Because the feature at 927 cm^{-1} is present in both thin films, we propose that this feature corresponds to the film environment at the solid−liquid interface, whereas the 950 cm^{-1} peak corresponds to the bulk. We believe the resulting uniformity of the liquid film is evidence of a similar transition in molecular ordering as observed for the dicyanamide ions shown in Figure 1. The possibility of a liquid to solid phase transition is eliminated by the consistent mobility of the liquid, as it continues to flow throughout the maturation process.

The two cyano-based ILs studied here display different favored orientation under the experimental conditions. Although $B(CN)_4$ favors the arrangement reported previously for a solid−liquid interface, $N(CN)_2$ adopts an orientation reported previously for the gas−liquid interface. This is interesting because in many other studies wherein the anions of the ILs remained the same, the substrate properties did not influence the liquid ordering behavior.[23] On the basis of the behavior we report here, the ion interactions with the metal versus gas phase, as well as intermolecular interactions within the liquid, are distinct and result in similar distinct organizations when allowed adequate time to mature.

CONCLUSIONS

Our studies of two cyano-based ILs supported in thin films show that the anions develop distinct chemical environments and adopt uniform molecular arrangements throughout the entire volume of the film. The symmetrical $B(CN)_4$ anion shows changes only in the B−C stretching peak. Because of the anion symmetry, we assign these changes to significant differences in a chemical environment of the film over time. Dicyanamide spectra display changes only in the cyanide anion features. The matured spectral profile is similar to SFG spectra observed in a previous study[33] of an IL with the same anion at the gas−liquid interface. The similarities of our thin film spectral profiles to these acquired exclusively of the interface imply the propagation of the gas−liquid interfacial assembly throughout the film in the case of P14 $N(CN)_2$, whereas the solid−liquid interfacial organization is favored in P14 $B(CN)_4$. The molecular arrangement in the matured films extends to 0.4 and 1.1 μm for $N(CN)_2$ and $B(CN)_4$, respectively. This is much thicker than previously reported interfacial film organization. The observation of a liquid templating the molecular organizations found at solid or gas interfaces, followed by development of long-ranging-ordered structures, is a promising avenue for controlling self-assembly in three dimensions, which will be beneficial for many important material applications.

ASSOCIATED CONTENT

Supporting Information

The Supporting Information is available free of charge on the ACS Publications website at DOI: 10.1021/acs.jpcc.8b12575.

Shift in the N−C asymmetric stretching peak as a function of film maturation; table of IL film maturation times and thicknesses; comparison of three spectra show no changes in the C≡N stretching peak of $B(CN)_4$; shift in peak frequencies as a function of time for two C≡N stretching modes for P14 $N(CN)_2$; shift in peak frequency as a function of time for B−C stretching mode for P14 $B(CN)_4$; IRRAS data for P14 $N(CN)_2$ and P14 $B(CN)_4$ films of variable dimension, proving IRRAS is sensitive to the entire film thickness (PDF)

AUTHOR INFORMATION

Corresponding Authors

*E-mail: radhikas-anaredy@uiowa.edu (R.S.A.).
*E-mail: scott-k-shaw@uiowa.edu (S.K.S.).

ORCID

Scott K. Shaw: 0000-0003-3767-3236

Notes

The authors declare no competing financial interest.

ACKNOWLEDGMENTS

The authors thank Dr. James Hilfiker at J.A. Woollam for his helpful discussions and assistance. We also thank Andrew Horvath (Shaw group) for acquiring IRRAS data at varying speeds of rotation. We also acknowledge excellent service and craftsmanship from the electronics, glass, and machining shops

DOI: 10.1021/acs.jpcc.8b12575
J. Phys. Chem. C 2019, 123, 8975−8982

at the University of Iowa, without that this work would not have been possible. Funding for this research was provided by the National Science Foundation via award no. 1651381 and the Research Corporation for Scientific Advancement for funding via the Cottrell Scholar Award. R.S.A. is grateful to the University of Iowa Graduate College for fellowship support during a portion of this work.

REFERENCES

(1) Rogers, R. D.; Seddon, K. R. CHEMISTRY: Ionic Liquids–Solvents of the Future? *Science* **2003**, *302*, 792.
(2) Johnson, K. E. What's an ionic liquid? *Electrochem. Soc. Interface* **2007**, *16*, 38−41.
(3) Krossing, I.; Slattery, J. M.; Daguenet, C.; Dyson, P. J.; Oleinikova, A.; Weingärtner, H. Why Are Ionic Liquids Liquid? A Simple Explanation Based on Lattice and Solvation Energies. *J. Am. Chem. Soc.* **2006**, *128*, 13427−13434.
(4) Amith, W. D.; Hettige, J. J.; Castner, E. W., Jr.; Margulis, C. J. Structures of Ionic Liquids Having Both Anionic and Cationic Octyl Tails: Lamellar Vacuum Interface vs Sponge-Like Bulk Order. *J. Phys. Chem. Lett.* **2016**, *7*, 3785−3790.
(5) Atkin, R.; Borisenko, N.; Drüschler, M.; Endres, F.; Hayes, R.; Huber, B.; Roling, B. Structure and Dynamics of The Interfacial Layer Between Ionic Liquids and Electrode Materials. *J. Mol. Liq.* **2014**, *192*, 44−54.
(6) Cooper, P. K.; Wear, C. J.; Li, H.; Atkin, R. Ionic Liquid Lubrication of Stainless Steel: Friction is Inversely Correlated with Interfacial Liquid Nanostructure. *ACS Sustainable Chem. Eng.* **2017**, *5*, 11737−11743.
(7) Sweeney, J.; Webber, G. B.; Rutland, M. W.; Atkin, R. Effect of Ion Structure on Nanoscale Friction in Protic Ionic Liquids. *Phys. Chem. Chem. Phys.* **2014**, *16*, 16651−16658.
(8) Hettige, J. J.; Araque, J. C.; Margulis, C. J. Bicontinuity and Multiple Length Scale Ordering in Triphilic Hydrogen-Bonding Ionic Liquids. *Journal of Physical Chemistry B* **2014**, *118*, 12706−12716.
(9) Russina, O.; Triolo, A.; Gontrani, L.; Caminiti, R. Mesoscopic Structural Heterogeneities in Room-Temperature Ionic Liquids. *J. Phys. Chem. Lett.* **2011**, *3*, 27−33.
(10) Shen, Y.; Kennedy, D. F.; Greaves, T. L.; Weerawardena, A.; Mulder, R. J.; Kirby, N.; Song, G.; Drummond, C. J. Protic Ionic Liquids with Fluorous Anions: Physicochemical Properties and Self-Assembly Nanostructure. *Phys. Chem. Chem. Phys.* **2012**, *14*, 7981−7992.
(11) Zheng, W.; Mohammed, A.; Hines, L. G., Jr.; Xiao, D.; Martinez, O. J.; Bartsch, R. A.; Simon, S. L.; Russina, O.; Triolo, A.; Quitevis, E. L. Effect of Cation Symmetry on the Morphology and Physicochemical Properties of Imidazolium Ionic Liquids. *Journal of Physical Chemistry B* **2011**, *115*, 6572−6584.
(12) Triolo, A.; Russina, O.; Bleif, H.-J.; Di Cola, E. Nanoscale Segregation in Room Temperature Ionic Liquids. *Journal of Physical Chemistry B* **2007**, *111*, 4641−4644.
(13) Baldelli, S. Surface Structure at the Ionic Liquid−Electrified Metal Interface. *Acc. Chem. Res.* **2008**, *41*, 421−431.
(14) Atkin, R.; Borisenko, N.; Druschler, M.; El Abedin, S. Z.; Endres, F.; Hayes, R.; Huber, B.; Roling, B. An in situ STM/AFM and impedance spectroscopy study of the extremely pure 1-butyl-1-methylpyrrolidinium tris(pentafluoroethyl)trifluorophosphate/Au(111) interface: potential dependent solvation layers and the herringbone reconstruction. *Phys. Chem. Chem. Phys.* **2011**, *13*, 6849−6857.
(15) Baldelli, S. Interfacial Structure of Room-Temperature Ionic Liquids at the Solid−Liquid Interface as Probed by Sum Frequency Generation Spectroscopy. *J. Phys. Chem. Lett.* **2013**, *4*, 244−252.
(16) Gong, X.; Frankert, S.; Wang, Y.; Li, L. Thickness-Dependent Molecular Arrangement and Topography of Ultrathin Ionic Liquid Films on a Silica Surface. *Chem. Commun.* **2013**, *49*, 7803−7805.
(17) Gong, X.; Kozbial, A.; Li, L. What Causes Extended Layering of Ionic Liquids on the Mica Surface? *Chem. Sci.* **2015**, *6*, 3478−3482.
(18) Akbulut, M.; Chen, N.; Maeda, N.; Israelachvili, J.; Grunewald, T.; Helm, C. A. Crystallization in Thin Liquid Films Induced by Shear. *Journal of Physical Chemistry B* **2005**, *109*, 12509−12514.
(19) Gee, M. L.; McGuiggan, P. M.; Israelachvili, J. N.; Homola, A. M. Liquid to solidlike transitions of molecularly thin films under shear. *J. Chem. Phys.* **1990**, *93*, 1895−906.
(20) Van Alsten, J.; Granick, S. Molecular Tribometry of Ultrathin Liquid Films. *Phys. Rev. Lett.* **1988**, *61*, 2570−2573.
(21) Ueno, K.; Kasuya, M.; Watanabe, M.; Mizukami, M.; Kurihara, K. Resonance Shear Measurement of Nanoconfined Ionic Liquids. *Phys. Chem. Chem. Phys.* **2010**, *12*, 4066−4071.
(22) Perkin, S.; Albrecht, T.; Klein, J. Layering and Shear Properties of an Ionic Liquid, 1-Ethyl-3-Methylimidazolium Ethylsulfate, Confined to Nano-Films Between Mica Surfaces. *Phys. Chem. Chem. Phys.* **2010**, *12*, 1243−1247.
(23) Anaredy, R. S.; Shaw, S. K. Long-Range Ordering of Ionic Liquid Fluid Films. *Langmuir* **2016**, *32*, 5147−5154.
(24) Bovio, S.; Podestà, A.; Lenardi, C.; Milani, P. Evidence of Extended Solidlike Layering in [Bmim][NTf2] Ionic Liquid Thin Films at Room-Temperature. *Journal of Physical Chemistry B* **2009**, *113*, 6600−6603.
(25) Gong, X.; Kozbial, A.; Rose, F.; Li, L. Effect of $\pi-\pi$+ Stacking on the Layering of Ionic Liquids Confined to an Amorphous Carbon Surface. *ACS Appl. Mater. Interfaces* **2015**, *7*, 7078−7081.
(26) Jurado, L. A.; Kim, H.; Arcifa, A.; Rossi, A.; Leal, C.; Spencer, N. D.; Espinosa-Marzal, R. M. Irreversible Structural Change of a Dry Ionic Liquid Under Nanoconfinement. *Phys. Chem. Chem. Phys.* **2015**, *17*, 13613−13624.
(27) Comtet, J.; Niguès, A.; Kaiser, V.; Coasne, B.; Bocquet, L.; Siria, A. Nanoscale Capillary Freezing of Ionic Liquids Confined Between Metallic Interfaces and The Role of Electronic Screening. *Nat. Mater.* **2017**, *16*, 634−639.
(28) Shin, J. Y.; Yamada, S. A.; Fayer, M. D. Dynamics of a Room Temperature Ionic Liquid in Supported Ionic Liquid Membranes vs the Bulk Liquid: 2D IR and Polarized IR Pump−Probe Experiments. *J. Am. Chem. Soc.* **2016**, *139*, 311−323.
(29) Nishida, J.; Breen, J. P.; Wu, B.; Fayer, M. D. Extraordinary Slowing of Structural Dynamics in Thin Films of a Room Temperature Ionic Liquid. *ACS Cent. Sci.* **2018**, *4*, 1065−1073.
(30) Kuang, D.; Wang, P.; Ito, S.; Zakeeruddin, S. M.; Grätzel, M. Stable Mesoscopic Dye-Sensitized Solar Cells Based on Tetracyanoborate Ionic Liquid Electrolyte. *J. Am. Chem. Soc.* **2006**, *128*, 7732−7733.
(31) Marszalek, M.; Fei, Z.; Zhu, D.-R.; Scopelliti, R.; Dyson, P. J.; Zakeeruddin, S. M.; Grätzel, M. Application of Ionic Liquids Containing Tricyanomethanide [C(CN)3]− or Tetracyanoborate [B(CN)4]− Anions in Dye-Sensitized Solar Cells. *Inorg. Chem.* **2011**, *50*, 11561−11567.
(32) MacFarlane, D. R.; Forsyth, S. A.; Golding, J.; Deacon, G. B. Ionic Liquids Based on Imidazolium, Ammonium and Pyrrolidinium Salts of The Dicyanamide Anion. *Green Chem.* **2002**, *4*, 444−448.
(33) Peñalber, C. Y.; Grenoble, Z.; Baker, G. A.; Baldelli, S. Surface Characterization of Imidazolium-Based Ionic Liquids with Cyano-Functionalized Anions at the Gas-Liquid Interface Using Sum Frequency Generation Spectroscopy. *Phys. Chem. Chem. Phys.* **2012**, *14*, 5122−5131.
(34) Peñalber, C. Y.; Baker, G. A.; Baldelli, S. Sum Frequency Generation Spectroscopy of Imidazolium-Based Ionic Liquids with Cyano-Functionalized Anions at the Solid Salt−Liquid Interface. *Journal of Physical Chemistry B* **2013**, *117*, 5939−5949.
(35) Anaredy, R. S.; Shaw, S. K. Developing Distinct Chemical Environments in Ionic Liquid Films. *Journal of Physical Chemistry C* **2018**, 19731.
(36) Gottardi, S.; Müller, K.; Moreno-López Juan, C.; Yildirim, H.; Meinhardt, U.; Kivala, M.; Kara, A.; Stöhr, M. Cyano-Functionalized Triarylamines on Au(111): Competing Intermolecular versus Molecule/Substrate Interactions. *Adv. Mater. Interfaces* **2014**, *1*, 1300025.

DOI: 10.1021/acs.jpcc.8b12575
J. Phys. Chem. C 2019, 123, 8975−8982

(37) Müller, K.; Moreno-López Juan, C.; Gottardi, S.; Meinhardt, U.; Yildirim, H.; Kara, A.; Kivala, M.; Stöhr, M. Cyano-Functionalized Triarylamines on Coinage Metal Surfaces: Interplay of Intermolecular and Molecule−Substrate Interactions. *Chem. − Eur. J.* **2016**, *22*, 581−589.
(38) Smoliński, S.; Zelenay, P.; Sobkowski, J. Effect Of Surface Order on Adsorption of Sulfate Ions on Silver Electrodes. *J. Electroanal. Chem.* **1998**, *442*, 41−47.
(39) *CRC Handbook of Chemistry and Physics*; 89 ed.; CRC press: Florida, 2009.
(40) Nania, S. L.; Shaw, S. K. Structural Changes in Acetophenone Fluid Films as a Function of Nanoscale Thickness. *Langmuir* **2017**, *33*, 1623−1628.
(41) Mao, J. X.; Lee, A. S.; Kitchin, J. R.; Nulwala, H. B.; Luebke, D. R.; Damodaran, K. Interactions in 1-ethyl-3-methyl imidazolium tetracyanoborate ion pair: Spectroscopic and Density Functional Study. *J. Mol. Struct.* **2013**, *1038*, 12−18.
(42) Majumder, A.; Pilet, G.; Garland Rodriguez, M. T.; Mitra, S. Synthesis and Structural Characterisation of Three Dicyanamide Complexes with Mn(II), Zn(II) and Cd(II): Supramolecular Architectures Stabilised by Hydrogen Bonding. *Polyhedron* **2006**, *25*, 2550−2558.
(43) Simons, T. J.; Howlett, P. C.; Torriero, A. A. J.; MacFarlane, D. R.; Forsyth, M. Electrochemical, Transport, and Spectroscopic Properties of 1-Ethyl-3-methylimidazolium Ionic Liquid Electrolytes Containing Zinc Dicyanamide. *Journal of Physical Chemistry C* **2013**, *117*, 2662−2669.
(44) Hayes, R.; Warr, G. G.; Atkin, R. Structure and Nanostructure in Ionic Liquids. *Chem. Rev.* **2015**, *115*, 6357−6426.
(45) Gong, X.; Wang, B.; Li, L. Spreading of Nanodroplets of Ionic Liquids on the Mica Surface. *ACS Omega* **2018**, *3*, 16398−16402.

DOI: 10.1021/acs.jpcc.8b12575
J. Phys. Chem. C 2019, 123, 8975−8982